Microstructure-based failure surfaces of matrix-inclusion materials: the origin of J_3 plasticity highlighted by limit analysis

J. Füssl[1] and R. Lackner[1,2]
[1] *Institute for Mechanics of Materials and Structures, Vienna University of Technology, Vienna, Austria*
[2] *Computational Mechanics, Technical University of Munich, Munich, Germany*

ABSTRACT: Composites composed of two materials, exhibiting a matrix-particle morphology, can be described by three phases: the matrix phase, the particle phase, and the interface between the particle and the matrix. In order to relate macroscopic material properties to the matrix-particle behavior and the morphology (material microstructure), analytical and/or numerical schemes may be employed. As regards macroscopic strength properties, averaging schemes as e.g. used for upscaling of elastic and viscoelastic properties are not able to capture the localized mode of material failure. In this paper, the application of a discretized form of the upper-bound theorem of limit analysis to upscaling of strength properties is proposed. By varying the loading situation on the microstructural representation of the material, microstructure-based macroscopic failure criteria are derived for different material morphologies. The presented upscaling scheme illustrates the influence of the particle content, the particle strength, and the interface degradation on the macroscopic failure criterion.

1 INTRODUCTION

In order to explain and, finally, predict the strength-determining processes in composite materials, appropriate methods for relating the macroscopic strength properties to their finer-scale origin are required. Depending on the microstructure of the material (regular or randomly-distributed), two modes of establishing this relation (also referred to as "upscaling") may be distinguished:

- *Unit-cell approach:* If the material microstructure is characterized by the spatial variation of physical quantities which can be represented by a combination of local fluctuations at the level of the elementary cell and a drift of this elementary cell, the periodic media theory, representing the material microstructure by the so-called unit cell, may be employed.
- *RVE approach:* The effective media theory, on the other hand, is based on the introduction of a representative volume element (RVE), stipulating the separation of observation scales. The size of an RVE must be (i) considerably larger than the characteristic dimension of the material phases forming the material at the considered scale and (ii) significantly smaller than the material or material phase built up by the RVE.

For most materials exhibiting a matrix-inclusion morphology, which are in general obtained by mixing, pouring and, if necessary, compaction/densification, the irregular arrangement of the microstructure renders the RVE approach as appropriate. Hereby, the response of the considered RVE may be computed numerically or analytically. As regards the latter, averaging schemes based on continuum micromechanics may be employed for upscaling of elastic and viscoelastic properties (see, e.g., (Aigner et al. 2007; Lackner and Mang 2006)). Recently, the range of application of continuum micromechanics was extended towards upscaling of strength properties, representing the elasto-plastic behavior of the material by a secant-elastic law (Lemarchand et al. 2002; Barthèlèmy and Dormieux 2004; Heukamp et al. 2005). Hereby, failure of the entire RVE is assumed. In general, however, material failure is characterized by the development of a localized failure zone, introducing a new length scale in the RVE (see Figure 1). As a remedy, the application of the discretized version of limit analysis, taking the localized character of material failure into account, is presented in this paper for upscaling of strength properties. First applications of limit analysis dealing with efficient non-linear solution algorithm were reported in (Zouain et al. 1993).

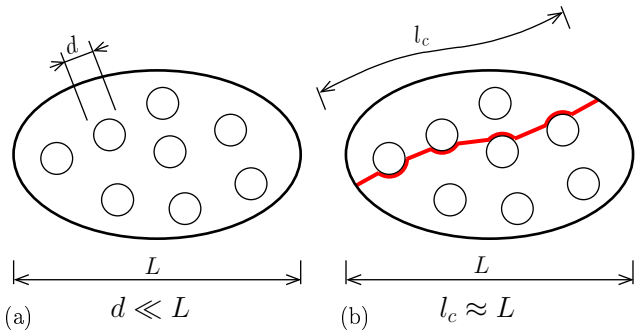

Figure 1. Separation of scales within RVE approach: (a) appropriate and (b) inappropriate configuration for upscaling by means of continuum micromechanics

In the following section, the discrete formulation of limit analysis for determination of upper bounds for failure loads following the work of (Krabbenhoft et al. 2005; Makrodimopoulos and Martin 2006) is briefly reviewed. The considered yield functions as well as their implementation as second-order-cone constraints within limit analysis is given in Section 3. The performance of the proposed upscaling scheme when applied to porous materials and matrix-particle materials is illustrated in Section 4.

2 DISCRETIZED FORM OF UPPER-BOUND LIMIT ANALYSIS

Originally, the objective of limit analysis was determination of the load-bearing capacity of structures exhibiting elastoplastic material response. At collapse, structures have exhausted their capacity to store any additional external work, $\dot{W}^{ext}$, as recoverable energy. For a given macroscopic strain-rate field $\dot{\mathbf{E}}(\mathbf{x})$ and a prescribed macroscopic stress field $\boldsymbol{\Sigma}(\mathbf{x})$, limit analysis concentrates on the critical rate of work, $\dot{W}^{ext} = \dot{W}^{int} = \boldsymbol{\Sigma} : \dot{\mathbf{E}}$, at failure (for the theoretical basis, see, e.g., (Ulm and Coussy 2003)). Hereby, $\boldsymbol{\Sigma} = \alpha\boldsymbol{\Sigma}_0$, where $\boldsymbol{\Sigma}_0$ defines the loading situation with α controls the load level. Accordingly, the problem is reduced to finding the limit value of α, α^*. The problem may be stated as follows: Find the admissible velocity field $\mathbf{u}(\mathbf{x}) \in \mathcal{U}$, which minimizes the internal dissipated energy $\dot{W}^{int}$ over the set of all statically admissible stress fields $\boldsymbol{\sigma}(\mathbf{x}) \in \mathcal{S}$, which maximize the internal dissipated energy $\dot{W}^{int}$. According to (Christiansen and Andersen 1999), the so-obtained saddle-point problem can be written as:

$$\alpha^* = \max\Big\{\alpha \mid \exists \boldsymbol{\sigma} \in \mathcal{S} \; : \; \dot{W}^{int}(\boldsymbol{\sigma}, \mathbf{u}) = \alpha \dot{W}^{ext}(\mathbf{u}) \quad \forall \mathbf{u} \in \mathcal{U}\Big\} \tag{1}$$

$$= \max_{\sigma \in \mathcal{S}} \min_{\substack{\mathbf{u}\in\mathcal{U} \\ \dot{W}^{ext}=1}} \dot{W}^{int}(\boldsymbol{\sigma}, \mathbf{u}) \tag{2}$$

$$= \min_{\substack{\mathbf{u}\in\mathcal{U} \\ \dot{W}^{ext}=1}} \max_{\sigma \in \mathcal{S}} \dot{W}^{int}(\boldsymbol{\sigma}, \mathbf{u}) \tag{3}$$

$$= \min_{\substack{\mathbf{u}\in\mathcal{U} \\ \dot{W}^{ext}=1}} \dot{D}(\mathbf{u}), \tag{4}$$

where $\dot{D} = \max_{\sigma\in\mathcal{S}} \dot{W}^{int}$ denotes the dissipation rate associated with the velocity field $\mathbf{u}$ [1]. Unfortunately, problem (1) to (4) can be solved only for simple geometric and loading situation and simple material behavior. For the case of a more complex situation, the plastic-flow compatibility ($\mathbf{u} \notin \mathcal{U}$) in the so-called static principle (Equation (1)), on the one hand, or the static equilibrium and the plastic admissibility ($\boldsymbol{\sigma} \notin \mathcal{S}$) in the so-called kinematic principle (Equation (4)), on the other hand, may be relaxed, providing access to lower and upper bounds for the limit multiplier α^*.

2.1 The kinematic approach – the upper-bound (UB) formulation

For the numerical UB formulation, 10-node tetrahedral linear-strain elements with plane sides and quadratic shape functions for the interpolation of the unknown velocity field are used. According to (Makrodimopoulos and Martin 2005b), linear strain elements show better performance in case of unstructured meshes than constant strain elements with velocity discontinuities. Moreover, if the vertices of the linear-strain elements are taken as the flow-rule points, the obtained solutions are strict upper bounds on the exact collapse load (Makrodimopoulos and Martin 2005a). For the stress field, a linear stress distribution is assumed within each element. To enforce the admissibility of the velocity-field solution within the UB formulation, the following conditions are imposed:

- The strain rate must follow an associative flow rule

$$\dot{\boldsymbol{\varepsilon}} = \dot{\lambda}\frac{\partial f}{\partial \boldsymbol{\sigma}}, \tag{5}$$

  where f denotes the yield function, $\dot{\boldsymbol{\varepsilon}}$ represents the strain-rate tensor, with $\dot{\varepsilon}_{ij} = 1/2\,(u_{i,j} + u_{j,i})$, and $\dot{\lambda}$ is the plastic multiplier, fulfilling $\dot{\lambda} \geq 0$.

- The velocity field has to fulfill the boundary conditions prescribed at the boundaries of the considered volume element (VE). As shown in Figure 2, only an eighth of an air void/particle is considered, with the normal velocity $u_n = 0$ on each symmetric plane. The outside planes of the

[1] The proof for the step from Equation (2) to Equation (3) can be found in (Christiansen 1996).

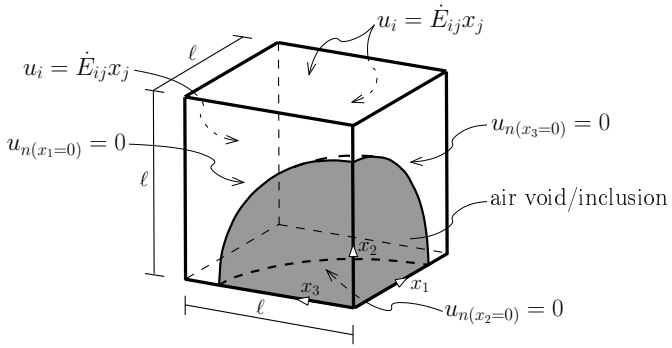

Figure 2. Considered VE, and applied velocity boundary conditions

VE, i.e., $A_1(x_1 = \ell, x_2, x_3)$, $A_2(x_1, x_2 = \ell, x_3)$, and $A_3(x_1, x_2, x_3 = \ell)$, are subjected to linear velocity boundary conditions $u_i = \dot{E}_{ij}x_j$ (with $\dot{E}_{ij} = 0$ for $i \neq j$), giving the macroscopic strain rates $\dot{E}_{ij}$ as the averages of the microscopic strain rates $\dot{\varepsilon}_{ij}$.

– Moreover, the rate of flow of material through the boundary A_i, with $i = 1, 2, 3$, is set to a prescribed value ζ_i.

Under these conditions, the internal rate of work

$$\dot{W}^{int} = \sum_{e=1}^{n_e} \int_{V^e} \left(\dot{\lambda} \frac{\partial f}{\partial \boldsymbol{\sigma}^T} \boldsymbol{\sigma} \right)^e dV \tag{6}$$

needs to be minimized, where n_e is the number of elements used to discretize the VE depicted in Figure 2. The dual to the respective upper-bound optimization problem $\min_{\mathbf{u} \in \mathcal{U}, \dot{W}^{ext}=1} \dot{W}^{int}$ is given by (Krabbenhoft, Lyamin, Hjiaj, and Sloan 2005):

$$\max \quad \alpha \tag{7}$$

$$\text{subject to} \quad \mathbf{B}^T \mathbf{q}_\sigma = \alpha \left\{ \begin{array}{c} \zeta_1 \mathbf{p}_1 \\ \zeta_2 \mathbf{p}_2 \\ \zeta_3 \mathbf{p}_3 \end{array} \right\} \tag{8}$$

$$\mathbf{f}(\mathbf{q}_\sigma) \leq 0 \tag{9}$$

where

$$\mathbf{B} = \int_{VE} \mathbf{N}_\sigma^T \nabla \mathbf{N}_u \, dVE \;\text{ and }\; \mathbf{p}_i = \int_{A_i} \mathbf{N}_u^T \mathbf{t} \, dA_i. \tag{10}$$

$\mathbf{N}_\sigma$ and $\mathbf{N}_u$ contain the interpolation functions for the quadratic velocity field and the linear stress field, respectively. $\mathbf{t}$ is a set of predefined external loads and $\mathbf{q}_\sigma$ is the vector of unknown nodal stresses. The yield condition $f(\mathbf{q}_\sigma) \leq 0$ is enforced at each corner node of an element and, thus, is satisfied throughout the whole element.

The solution of this upper-bound optimization problem in the framework of cone-programming is described in detail in the following section.

3 FAILURE CRITERIA AND SOLUTION OF OPTIMIZATION PROBLEM

The optimization problem (7) to (9) is nonlinear, with the nonlinearity introduced by the yield functions $f(\mathbf{q}_\sigma)$. Thus, if the yield function is convex, the optimization problem itself is convex and there exists only one optimum which is the global optimum. In recent years, different nonlinear-convex optimization strategies were applied to limit-analysis problems: In (Lyamin and Sloan 2002), a Two-Stage-Quasi-Newton algorithm is employed by linearizing the optimality conditions and solving the resulting linear system iteratively. In (Krabbenhoft and Damkilde 2003), another interior point method based on the logarithmic barrier function is used. Furthermore, a sequential-quadratic-programming scheme may be used to solve the underlying quadratic optimization problem by the primal-dual interior point solver described in (Gondzio 1995). In case of yield surfaces exhibiting corners and edges and, thus, becoming non-differentiable, smoothing of the yield surface was proposed in (Abbo and Sloan 1995). In case of cone-shaped yield criteria (such as, e.g., the Mohr-Coulomb criterion in plane strain and the Drucker-Prager criterion in 2D and 3D), second-order-cone-programming (SOCP) was successfully used in (Makrodimopoulos and Martin 2006). Hereby, the conic optimization problem [2] is solved efficiently by an interior point method. In this paper, the algorithm outlined in (Andersen et al. 2003), which has been implemented in MOSEK (ApS 2006), is used. Hereby, yield criterion has the form

$$f(\mathbf{q}_\sigma) = \sqrt{\mathbf{q}_\sigma^T \mathbf{M} \mathbf{q}_\sigma} + \mathbf{m}^T \mathbf{q}_\sigma - k \leq 0, \tag{15}$$

[2] A general conic optimization problem consists of a linear objective function

$$\min \left\{ \mathbf{c}^T \mathbf{x} \right\}, \quad \text{with} \quad \mathbf{x} \in \mathbf{R}^n, \tag{11}$$

subjected to (i) a set of linear constraints $\mathbf{Ax} = \mathbf{b}$ and (ii) the conic constraints $\mathbf{x} \in \mathcal{C}$, where $\mathcal{C}$ is a closed convex pointed cone. A set $\mathcal{C}$ is called a cone if $\forall \mathbf{x} \in \mathcal{C}$ and $\lambda \geq 0$, $\lambda \mathbf{x} \in \mathcal{C}$. Examples of such cones are

– the nonnegative orthant

$$\mathcal{C} = \mathcal{R}_+ = \{x : x \geq 0\}, \tag{12}$$

– the second-order (or ice-cream) cone

$$\mathcal{C} = \left\{ \mathbf{x} \in \mathcal{R}^m : \sqrt{\sum_{i=2}^{m} x_i^2} \leq x_1, x_1 \geq 0 \right\}, \tag{13}$$

– and the rotated quadratic cone

$$\mathcal{C} = \left\{ \mathbf{x} \in \mathcal{R}^m : \sum_{i=3}^{m} x_i^2 \leq 2 x_1 x_2, x_1 \geq 0, x_2 \geq 0 \right\}. \tag{14}$$

or, equivalently,

$$\sqrt{\mathbf{q}_\sigma^T \mathbf{M} \mathbf{q}_\sigma} \leq k - \mathbf{m}^T \mathbf{q}_\sigma, \tag{16}$$

where $\mathbf{M}$ is at least positive semi-definite. The cone formulation of Equation (16) is obtained by introducing (Makrodimopoulos 2006)

$$\mathbf{M} = \mathbf{L}^T \mathbf{L}, \quad \mathbf{y} = \mathbf{L}\mathbf{q}_\sigma, \quad \text{and} \quad z = k - \mathbf{m}^T \mathbf{q}_\sigma, \tag{17}$$

giving

$$\sqrt{\mathbf{y}^T \mathbf{y}} \leq z, \tag{18}$$

where $\mathbf{L} \in R^{h \times d}$ ($h = \text{rank}(\mathbf{M})$, $d =$ dimension of $\mathbf{q}_\sigma$) and $\mathbf{y}$ and z are auxiliary variables.

For the UB calculations presented in this paper, the Drucker-Prager criterion is used, reading

$$f(\boldsymbol{\sigma}) = \sqrt{\frac{1}{2} s_{ij} s_{ij}} + a\sigma_m - k, \tag{19}$$

with

$$\sigma_m = \frac{1}{3}(\sigma_{11} + \sigma_{22} + \sigma_{33}) \text{ and } s_{ij} = \sigma_{ij} - \sigma_m \delta_{ij}, \tag{20}$$

where s_{ij} is the stress deviator, σ_m is the mean stress, and a and k are the strength parameters. The quantities of the respective cone formulation (17) read

$$\mathbf{L} = \begin{bmatrix} 1 & 1/2 & 0 & 0 & 0 \\ 0 & \sqrt{3}/2 & 0 & 0 & 0 \\ 0 & 0 & 1 & 0 & 0 \\ 0 & 0 & 0 & 1 & 0 \\ 0 & 0 & 0 & 0 & 1 \end{bmatrix}, \quad \mathbf{y} = \begin{Bmatrix} y_1 \\ y_2 \\ y_3 \\ y_4 \\ y_5 \end{Bmatrix}, \tag{21}$$

$$\mathbf{q}_\sigma = \begin{Bmatrix} s_{11} \\ s_{22} \\ s_{12} \\ s_{13} \\ s_{23} \end{Bmatrix}, \quad \text{and} \quad z = k - a\sigma_m. \tag{22}$$

4 UB THEOREM APPLIED TO HETEROGENEOUS MATERIALS

In this section, the application of the UB theorem of limit analsysis in the context of upscaling of strength properties is presented. For this purpose, the material system illustrated in Figure 3, consisting of an eighth of an air void or particle, respectively, the matrix material and the interface between matrix and particle, is discretized. The three outside planes of the VE are subjected to different velocities $\zeta_i \mathbf{p}_i^T \dot{\mathbf{u}}_i$, with $i = 1, 2, 3$, giving access to respective macroscopic stress states at collapse, $\boldsymbol{\Sigma}$. All three material phases obey the Drucker-Prager failure criterion, with the strength properties a and k characterizing the internal friction angle of the material and the limit in pure shear, respectively. Different strength properties are assigned to the matrix (a_m and k_m), the particle (a_p and k_p), and the interface (a_I and k_I). By means of limit analysis, upper bounds for the material strength are computed for different loading situations.

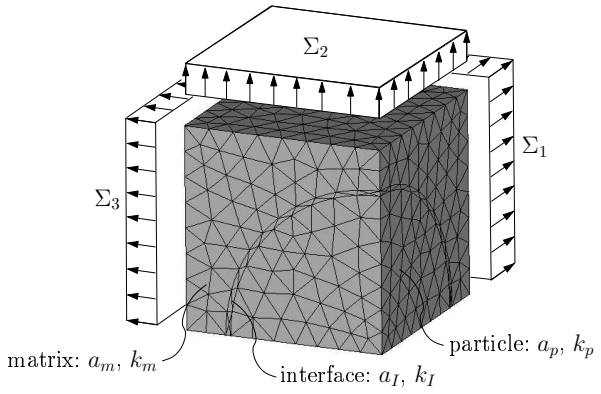

Figure 3. Illustration of the discretization of the considered VE for the application of the UB theorem

4.1 Porous material

To assess the accuracy of the discretization and the influence of the mesh type, a porous material subjected to uniaxial tension (Figure 4, disordered mesh) is investigated. Figure 4 shows upper bounds of the tensile strength for two different mesh types (mapped and disordered) as a function of the number of tetrahedral elements. According to Figure 4, the influence of the mesh type on the tensile strength is small. Moreover, the change in the result become rather small for element numbers higher than 2000. Thus, for the calculations presented within this paper, disordered meshes with 2000 to 3000 elements are used.

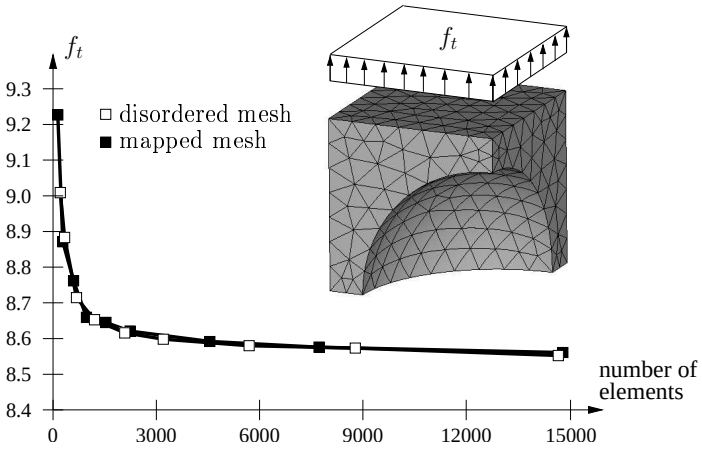

Figure 4. Upper bound for tensile strength f_t as a function of number of tetrahedral elements for a mapped and a disordered mesh ($f_a = 27\%$, $a_m = 0.35$, and $k_m = 10$)

In (Barthèlèmy and Dormieux 2003), a macroscopic failure criterion for porous materials was derived from nonlinear homogenization techniques (effective strain approach) in the framework of poromechanics, reading

$$f(\boldsymbol{\Sigma}) = \left(\frac{3f_a}{4} - a^2\right)\Sigma_m^2 + \left(1 + \frac{2}{3}f_a\right)\Sigma_d^2 + 2a^2 h(1 - f_a)\Sigma_m - a^2 h^2 (1 - f_a)^2, \tag{23}$$

where Σ_m and Σ_d are the macroscopic mean and deviatoric stress invariants, respectively, f_a is the air-void content, and $h = k/a$. As illustrated in Figure 5, the macroscopic criterion (23) agrees well to the UB result for a strength parameter a of 0.1. However, with

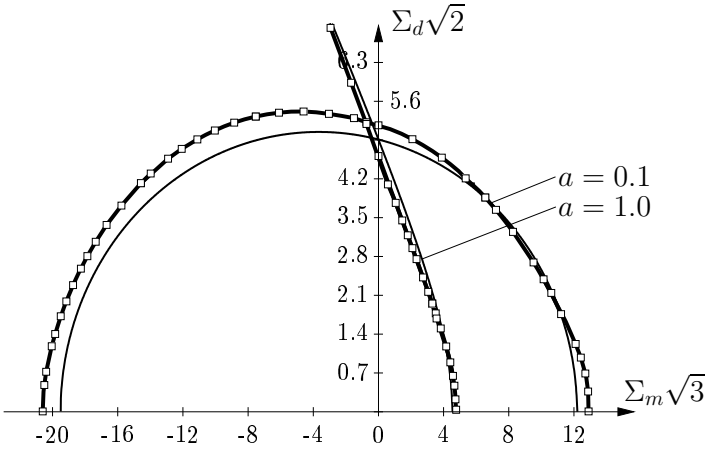

Figure 5. UB of macroscopic failure criterion of a porous material compared to the analytically-derived failure criterion (23) ($f_a = 25\%$ and $k = 5$)

increasing strength parameter a, the failure criterion (23) overestimates the strength of the porous material in the compressive loading regime (see Figure 6). (see also (Trillat, Pastor, and Thorè 2006)). For val-

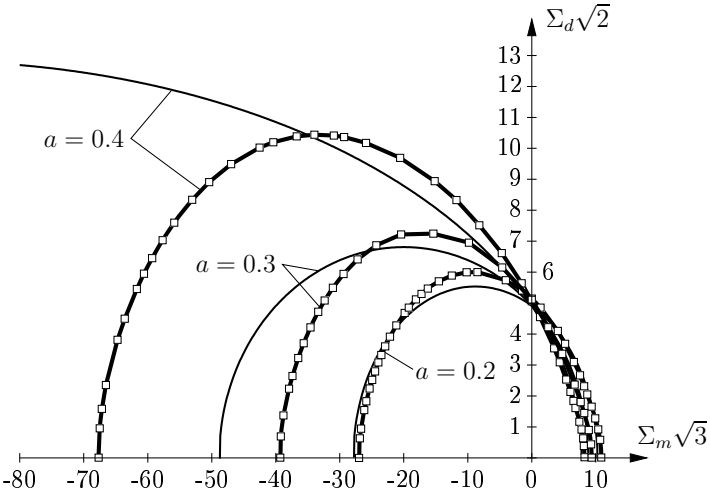

Figure 6. UB of macroscopic failure criterion of a porous material compared to the analytically-derived failure criterion (23) for different values of a ($f_a = 25\%$ and $k = 5$)

ues of a larger than $\sqrt{3f_a/4} = 0.43$, with $f_a = 25\%$, the first term of the failure criterion (23) becomes negative. Thus, in contrast to the UB result, failure becomes impossible in the hydrostatic compressive loading regime (see Figure 7).

4.2 Matrix-particle materials

In the following, two-phase materials, consisting of a particle with the strength properties a_p and k_p sur-

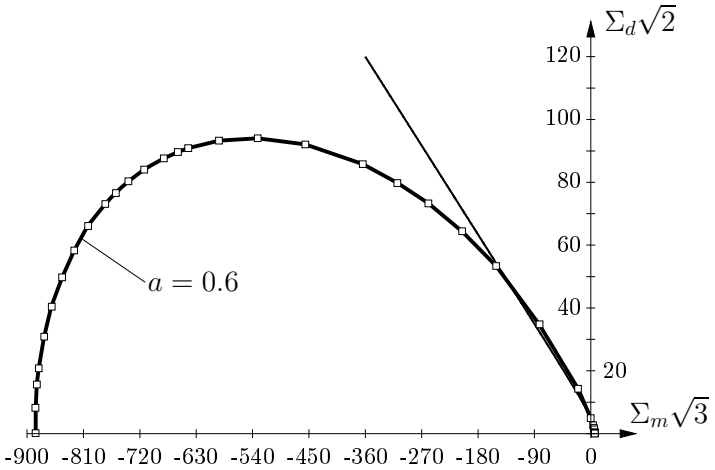

Figure 7. UB of macroscopic failure criterion of a porous material compared to the analytically-derived failure criterion (23) ($f_a = 25\%$, $a = 0.6$, and $k = 5$)

rounded by a matrix with the strength properties a_m and k_m, are investigated (see Figure 3).

Figure 8 contains upper bounds of the uniaxial tensile strength as a function of the ratio k_p/k_m, ranging from 1 to 7, and for three different particle contents. The obtained results show that the reinforcing effect of the particle increases with increasing particle content and increasing strength ratio k_p/k_m. However, at a certain strength ratio, failure occurs exclusively in the matrix phase and no further increase of the tensile strength is observed for increasing particle strength.

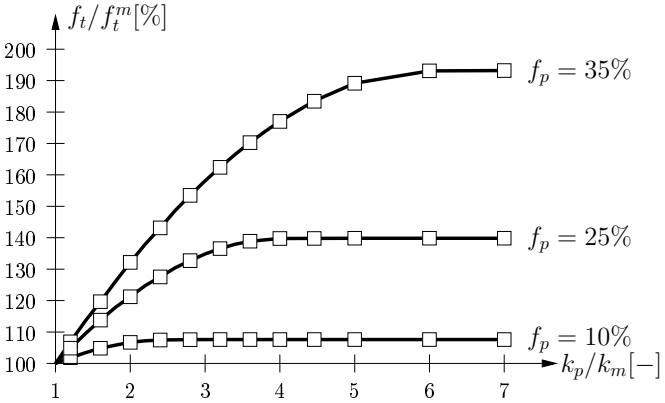

Figure 8. UB of uniaxial tensile strength as a function of the particle/matrix-strength ratio k_p/k_m for different values of f_p ($a_p = a_m = 0.1$)

Figure 9 shows upper bounds of 3D (macroscopic) failure surfaces of matrix-particle materials with rigid particles. Three different particle contents are investigated and the results for two different Lode angle ϑ are plotted in the (Σ_m/Σ_d)-plane. The strength parameter a of the macroscopic failure surface, which is related to the slope of the failure criterion in the (Σ_m/Σ_d)-plane, increases with increasing particle content f_p. The parameter h, with $h = k/a$, on the other hand, is not affected by the addition of particles. h defines the location of the failure surface on the hydrostatic axis ($\Sigma_d = 0$) and is equal to h of the matrix

material, with $h_m\sqrt{3} = k_m/a_m\sqrt{3} = 86.6$. Figure 10

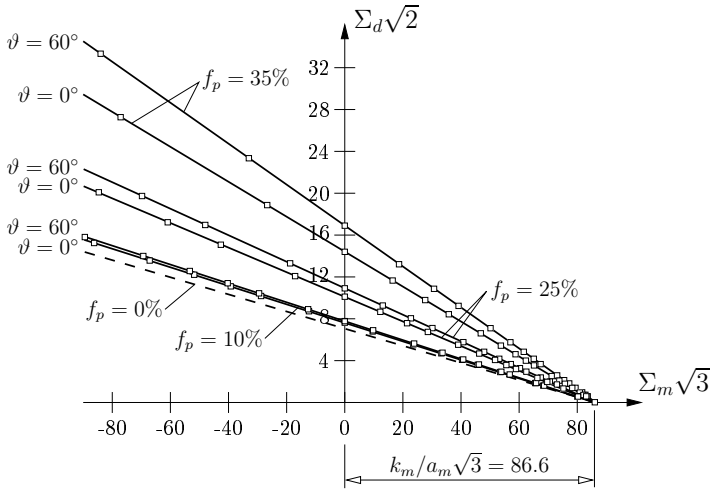

Figure 9. UB of macroscopic failure surfaces of matrix-particle materials for different values of f_p and rigid particles ($a_m = 0.1$ and $k_m = 5$)

shows the macroscopic failure surface in the deviatoric plane for $\Sigma_m = 0$. As a result of the particle, the rotational symmetry of the Drucker-Prager failure surface assigned to the matrix material is lost. Macroscopic stress states, characterized by $\vartheta = 60°$ (compressive meridian), lead to a higher material strength than stress states located on the tensile meridian ($\vartheta = 0°$). This out-of-roundness effect increases with increasing particle content and decreasing mean stress (see Figures 9 and 10). The resulting failure surface can be approximated with three ellipses, which is consistent with frequently obtained failure criteria derived from experimental data for different composite materials (see, e.g., (Launay and Gachon 1972; Mills and Zimmerman 1970)).

In the previous studies, a perfect bond between the matrix and the particle was assumed. In fact, failure of matrix-particle materials is often influenced by degraded interfaces between the matrix and the particles. For this purpose, we extended the considered VE by introducing a thin interface zone (see Figure 3), with the strength properties a_I and k_I. The possibility of reducing the strength properties of the interface allows consideration of debonding between particles and the matrix during upscaling. Figure 11 shows upper bounds for the 3D failure surface of a matrix-particle material with degraded and non-degraded interface, respectively. Hereby, failure of the interface is described by the Drucker-Prager criterion, with $k_I = 0.4k_m$ and $a_I = a_m$. For positive mean stress Σ_m, the material strength becomes lower than the strength of the pure matrix material. The largest reduction of the material strength (about 50%) is obtained for pure hydrostatic tensile loading. Figure 12 shows the deviatoric plane for $\Sigma_m = 0$ of the macroscopic failure surface of a material with degraded and non-degraded interface, respectively.

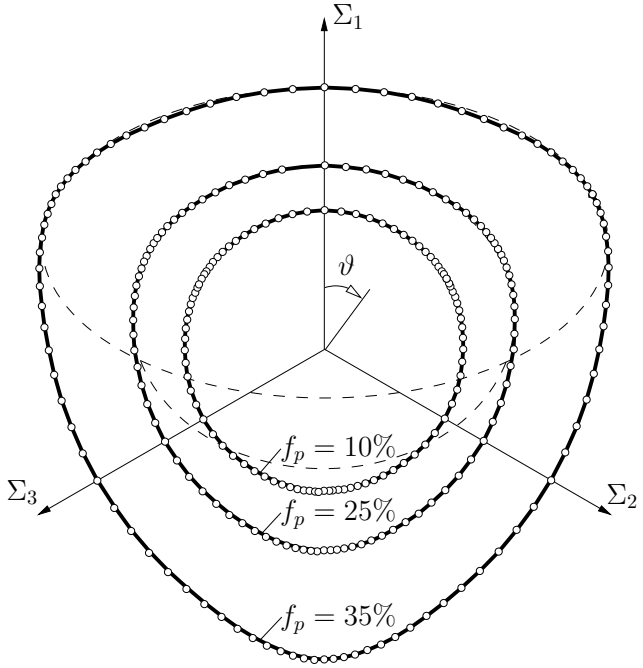

Figure 10. UB of macroscopic failure surface in deviatoric plane at $\Sigma_m = 0$ for different values of f_p ($a_m = 0.1$ and $k_m = 5$)

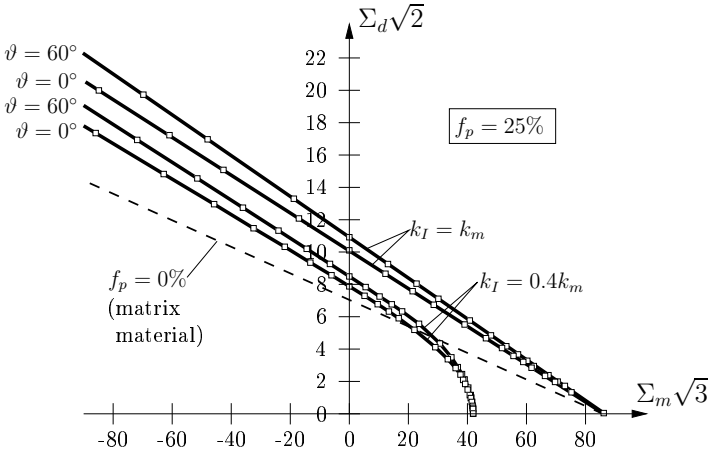

Figure 11. Influence of degraded interface ($k_I = 0.4k_m$) on UB of macroscopic failure surface ($f_p = 25\%$, $a_m = 0.1$, and $k_m = 5$)

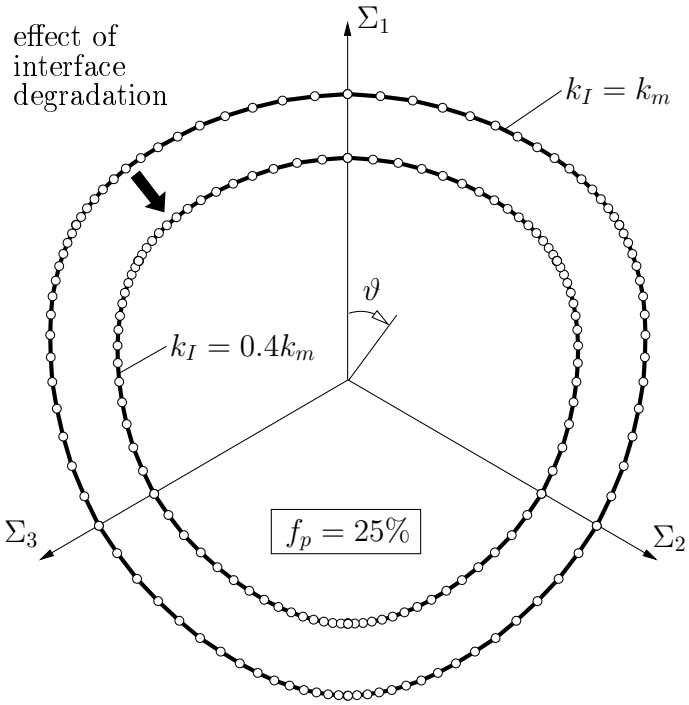

Figure 12. UB of macroscopic failure surface in deviatoric plane at $\Sigma_m = 0$ for a material with degraded/non-degraded interface ($f_p = 25\%$, $a_m = 0.1$, and $k_m = 5$)

5 CONCLUSIONS

In this paper, numerical upper-bound (UB) limit-analysis was proposed for upscaling of material strength properties, suitable for capturing complex mechanisms as observed in matrix-inclusion materials. The performance of the proposed upscaling technique was illustrated by different investigations, focusing on the effect of air voids and particles, and of the degradation of interface properties on the (macroscopic) material strength. Based on the obtained results, the following conclusions can be drawn:

- While good agreement was obtained between the analytically-derived failure criterion for porous materials (Barthèlèmy and Dormieux 2003) and the UB results in the tensile and deviatoric loading regime, the analytically-derived failure criterion overestimates the strength of the porous material in case of predominant compressive loading.

- In case of intact interfaces between particles and the matrix, the presence of particles lead to an improvement of strength properties of the composite material. Interestingly, this improvement, which is higher for increasing strength properties of the particles, remains constant for a particle-matrix strength ratio k_p/k_m higher than a certain threshold value. In fact, for these strength ratios, failure occurs exclusively in the matrix phase.

- The obtained macroscopic failure surface for matrix-particle materials exhibits an out-of-roundness in the deviatoric stress plane. This is in excellent agreement with failure surfaces derived from experimental data.

- The degradation of strength properties at the interface between particles and matrix, an often-observed phenomenon in matrix-particle materials, resulted in a significant drop of strength properties of the composite material. The aforementioned improvement of strength properties due to the presence of particles was compensated by the degradation process, especially for loading states characterized by a positive mean stress.

REFERENCES

Abbo, A. and S. Sloan (1995). A smoothed hyperbolic approximation to the Mohr-Coulomb yield criterion. *Computers and Structures 54*, 427–441.

Aigner, E., R. Lackner, and C. Pichler (2007). Micromechanics-based determination of viscous properties of asphalt concrete. *Journal of Materials in Civil Engineering (ASCE)*. Submitted for publication.

Andersen, E., C. Roos, and T. Terlaky (2003). On implementing a primal-dual interior-point method for conic quadratic optimization. *Mathematical Programming, Series B 95*, 249–277.

ApS, M. (2006). The MOSEK optimization tools version 4.0 (revision 35). *User's Manual and Reference, available from http://www.mosek.com*.

Barthèlèmy, J. and L. Dormieux (2003). Dètermination du critère de rupture macroscopique d'un milieu poreux par homogènèisation non linèaire. *C.R.Mècanique*, 271–276.

Barthèlèmy, J. and L. Dormieux (2004). A micromechanical approach to the strength criterion of Drucker-Prager materials reinforced by rigid inclusions. *International Journal for Numerical an Analytical Methods in Geomechanics 28*, 565–582.

Christiansen, E. (1996). Limit analysis of collapse states. *In Handbook of Numerical Analysis 4*, 193–312.

Christiansen, E. and K. Andersen (1999). Computation of collapse states with von Mises type yield condition. *International Journal for Numerical Methods in Engineering 46*, 1185–1202.

Gondzio, J. (1995). HOPDM (version 2.12) – a fast LP solver based on a primal-dual interior point method. *European Journal of Operational Research 85*, 221–225.

Heukamp, F., E. Lemarchand, and F. Ulm (2005). The effect of interfacial properties on the cohesion of highly filled composite materials. *International Journal of Solids and Structures 42*, 287–305.

Krabbenhoft, K. and L. Damkilde (2003). A general non-linear optimization algorithm for lower bound limit analysis. *International Journal for Numerical Methods in Engineering 56*, 165–184.

Krabbenhoft, K., A. Lyamin, M. Hjiaj, and S. Sloan (2005). A new discontinuous upper bound limit analysis formulation. *International Journal for Numerical Methods in Engineering 63*(7), 1069–1088.

Lackner, R. and H. Mang (2006). *Mehrskalenmodelle für die Berechnung von Flächentragwerken [Multiscale models for the analysis of shell structures]*. Ernst und Sohn, Betonkalender 2007. In German., Band 2, 19–65.

Launay, P. and H. Gachon (1972). Strain and ultimate strength of concrete under triaxial stress. *ACI Special Publication 34*(13).

Lemarchand, E., F. Ulm, and L. Dormieux (2002). Effect of inclusions on friction coefficient of highly filled compsite materials. *Journal of Engineering Mechanics 128*(8), 876–884.

Lyamin, A. and S. Sloan (2002). Lower bound limit analysis using non-linear programming. *International Journal for Numerical Methods in Engineering 55*, 573–611.

Makrodimopoulos, A. (2006). Computational formulation of shakedown analysis as a conic quadratic optimization problem. *Mechanics Research Communications 33*, 72–83.

Makrodimopoulos, A. and C. Martin (2005a). Limit analysis using large-scale socp optimization. In *Proc. 13th Nat. Conf. of UK Association for Computational Mechanics in Engineering, Sheffield*, pp. 21–24.

Makrodimopoulos, A. and C. Martin (2005b). A novel formulation of upper bound limit analysis as a second-order cone programming problem. In *Proc. 8th Int. Conf. on Computational Plasticity, Barcelona*, Number 2, pp. 1083–1086.

Makrodimopoulos, A. and C. Martin (2006). Lower bound limit analysis of cohesive-frictional materials using second-order cone programming. *International Journal for Numerical Methods in Engineering 66*(4), 604–634.

Mills, L. and R. Zimmerman (1970). Compressive strength of plain concrete under multiaxial loading conditions. *ACI Journal 67*(10), 802–807.

Trillat, M., J. Pastor, and P. Thorè (2006). Limit analysis and conic programming: 'porous drucker-prager' material and gurson's model. *Comptes Rendus Mecanique 334*(10), 599–604.

Ulm, F. and O. Coussy (2003). *Mechanics and Durability of Solids, Volume I - Solid Mechanics*. MIT/Prentice Hall, Upper Saddle River, New Jersey.

Zouain, N., J. Herskovits, L. Borges, and R. Feijoo (1993). An iterative algorithm for limit analysis with nonlinear yield functions. *International Journal of Solids and Structures 30*(10), 1397–1417.